Published in final edited form as:
Arterioscler Thromb Vasc Biol. 2009 October ; 29(10): 1444–1451. doi:10.1161/ATVBAHA.109.193086.

Hybrid in vivo FMT-CT imaging of protease activity in atherosclerosis with customized nanosensors

Matthias Nahrendorf, MD, PhD[*,1,2], **Peter Waterman, BS**[*,1,2], **Greg Thurber, PhD**[1], **Kevin Groves, PhD**[3], **Milind Rajopadhye, PhD**[3], **Peter Panizzi, PhD**[1,2], **Brett Marinelli, BS**[1], **Elena Aikawa, MD PhD**[2], **Mikael J Pittet, PhD**[1,2], **Filip K Swirski, PhD**[1,2], and **Ralph Weissleder, MD, PhD**[1,2]

[1]Center for Systems Biology, Massachusetts General Hospital and Harvard Medical School, Simches Research Building, 185 Cambridge St., Boston, MA 02114

[2]Center for Molecular Imaging Research, Massachusetts General Hospital and Harvard Medical School, Building 149, 13th St., Charlestown, MA 02129

[3]VisEn Medical, Inc., 45 Wiggins Avenue, Bedford, MA 01730

Abstract

Corresponding author: Ralph Weissleder, MGH-CSB, CPZN-5206, 185 Cambridge Street, Boston, MA 02124, Tel: 617-726-8226, Fax: 617-643-6133, rweissleder@mgh.harvard.edu.
*These authors contributed equally

Author Disclosures

Matthias Nahrendorf:	
Research Grant:	American Heart Association, Amount: < $10,000
Peter Waterman:	
Ownership Interest:	Visen Medical, Amount: < $10,000
Greg Thurber: No disclosures	
Kevin Groves:	
Institution/Employer:	Visen Medical, Amount: >= $10,000
Milind Rajopadhye:	
Institution/Employer:	Visen Medical, Amount: >= $10,000
Peter Panizzi: No disclosures	
Brett Marinelli: No disclosures	
Elena Aikawa: No disclosures	
Mikael Pittet: No disclosures	
Filip Swirski: No disclosures	
Ralph Weissleder:	
Research Grant:	NIH grant, Amount: >= $10,000
Ownership Interest:	Visen Medical, Amount: >= $10,000
Consultant/Advisory Board:	Visen Medical, Amount: < $10,000

Conflict of Interest Disclosures
Kevin Groves and Millind Rajopadhye are employees of VisEn Medical. Ralph Weissleder is a consultant to VisEn Medical. Ralph Weissleder and Peter Waterman hold VisEn shares.

Objective—Proteases are emerging biomarkers of inflammatory diseases. In atherosclerosis, these enzymes are often secreted by inflammatory macrophages, digest the extracellular matrix of the fibrous cap and destabilize atheromata. Protease function can be monitored with protease activatable imaging probes and quantitated in vivo by fluorescence molecular tomography (FMT). To address two major constraints currently associated with imaging of murine atherosclerosis (lack of highly sensitive probes and absence of anatomical information), we compared protease sensors (PS) of variable size and pharmacokinetics and co-registered FMT datasets with computed tomography (FMT-CT).

Methods and results—Co-registration of FMT and CT was achieved with a multimodal imaging cartridge containing fiducial markers detectable by both modalities. A high-resolution CT angiography protocol accurately localized fluorescence to the aortic root of atherosclerotic apoE$^{-/-}$ mice. To identify suitable sensors, we first modeled signal kinetics in-silico and then compared three probes with identical oligo-L-lysine cleavage sequences: PS-5, 5nm in diameter containing 2 fluorochromes , PS-25, a 25nm version with an elongated lysine chain and PS-40, a polymeric nanoparticle. Serial FMT-CT showed fastest kinetics for PS-5 but, surprisingly, highest fluorescence in lesions of the aortic root for PS-40. PS-40 robustly reported therapeutic effects of atorvastatin, corroborated by ex vivo imaging and qPCR for the model protease cathepsin B.

Conclusions—FMT-CT is a robust and observer-independent tool for non-invasive assessment of inflammatory murine atherosclerosis. Reporter-containing nanomaterials may have unique advantages over small molecule agents for in vivo imaging.

Keywords

FMT-CT; molecular imaging; atherosclerosis; protease activity; inflammation

Introduction

A thin fibrous cap, presence of macrophages and foam cells, and increased activity of proteases are hallmarks of atherosclerotic lesions at risk for causing myocardial infarction and stroke.[1] Typically, the fibrous cap and the endothelial layer are damaged due to heightened inflammatory activity, thus exposing the thrombogenic plaque core to platelets and coagulation factors in the blood stream. This triggers thrombotic occlusion of the artery followed by ischemic injury of downstream tissue.[1] Positive remodeling of the artery may obscure detection of inflamed plaques as the vessel lumen can be virtually unchanged, while some protruding plaques that cause significant stenosis on angiography are fairly stable.[2] Hence, protease activity in a lesion may have a higher predictive value for ischemic events than reported for the anatomic degree of stenosis.[3]

Protease presence in atherosclerotic lesions has been imaged with radiolabeled small molecule inhibitors [4, 5] and more recently with a MRI detectable Gd chelate attached to an affinity peptide targeting MMPs.[6] Fluorescent protease sensors (PS), which are injected in an inactive form and only emit signal after cleavage of a peptide sequence specific to their target enzyme, have been used to image protease activity.[7] Cysteine proteases are mainly expressed by monocytes/macrophages,[8, 9] cells which orchestrate atherosclerotic lesion development and destabilization. They promote digestion of extracellular matrix, leukocyte transmigration, apoptosis and neovascularization in atheromata,[1, 10] and can thus serve as imaging biomarkers for plaques with a high risk of thrombotic complication.[11]

Fluorescence Molecular Tomography (FMT) is emerging as a quantitative modality for non-invasive whole mouse imaging,[12] and can be used to detect and quantitate inflammatory protease activity.[7, 13] High-throughput capabilities with scan times of <5 minutes, cost-effectiveness, high sensitivity, absence of radiation and simultaneous imaging of multiple

biomarkers in spectrally resolved channels are advantages that promote the use of FMT.[14] However, there are two challenges to more widespread application in imaging of murine atherosclerosis. First, similar as seen in stand-alone PET imaging of atherosclerosis, there is often a paucity of anatomic information in optical-only FMT data sets (unless additional imaging probes capable of reporting structural information are co-injected). Since atherosclerotic plaques are small and vary in distribution, their accurate localization in such data sets is challenging. To overcome this limitation, we have developed hybrid FMT-CT protocols, similarly as is done in combined PET-CT imaging.[15–17] Second, we address the lack of molecular probes with optimized signal- and pharmakokinetics for in vivo FMT imaging of atherosclerotic plaques. While the targeting strategy of PS has been validated,[8, 11] the influence of probe design on signal kinetics and sensitivity has not yet been investigated. In particular, size effects of nanoparticulate sensors have been less well studied. Based on in-silico modeling, we synthesized, characterized and compared three differently sized nano-sensors activated by cysteine proteases. To compare the attributes of PS that are different in design and size but share the cleavage peptide sequence that triggers their activation, we serially imaged atherosclerotic lesions in apoE$^{-/-}$ mice using non-invasive hybrid FMT-CT. We further investigated if the lead compound has the dynamic range and sensitivity to detect benchmark anti-atherosclerotic treatment with atorvastatin.

Methods

Agent synthesis

A schematic overview of agent design and mechanism of activation is given in Figure 1A–B. We combined the epsilon-protected lysine oligo-peptides (1.5 μmol, Tufts University Core) and VivoTag-S680 (Visen Medical) in 100 μL of N,N-dimethylformamide (DMF) with N-methylmorpholine (NMM) and N,N-dimethylaminopyridine (DMAP) to synthesize a fluorochrome labeled peptide (in the following termed FLP). The labeled peptide was isolated by centrifugation and purified by HPLC. For synthesis of PS-5, FLP was combined with mPEG-NH2. 1-Ethyl-3-(3-dimethylaminopropyl) carbodiimide hydrochloride and hydroxybenzotriazole were added to the solution. After deprotection of the epsilon-amine, crude PS-5 was purified by reversed phase HPLC and characterized by SEC HPLC. The 25 nm sized agent (PS-25) was formed by controlled precipitation in alkaline polymer solution. For synthesis of PS-40, we combined a solution of amine-functionalized polymeric nanoparticles[18] (~40 nm particles, ~200 amines / particle) in MES with 0.25 μmol of the above described fluorochrome labeled peptide. The nanoparticles were washed with ammonium bicarbonate and then purified by gel filtration chromatography using Biogel P100 (Biorad). Approximately 5–6 FLP were conjugated to each nanoparticle.

Target enzymes

To evaluate the target profile, we incubated PS-25 with a panel of enzymes including key proteases present in atherosclerotic plaques. PS-25 (0.5 mM) was mixed with enzymes (20 nM) in appropriate buffers at room temperature. The following enzymes were purchased from R&D, Sigma or Calbiochem: cathepsin B, D, G, K, L, S, plasmin, trypsin and uPA. Reaction progress was monitored at excitation/emission wavelengths of 663/691 using a Gemini-XS plate reader.

Modeling of in vivo sensor activation

A mechanistic model was developed for activation of differently sized PS and resulting fluorochrome concentrations in atherosclerotic plaque. Details of the model are provided in the supplemental information.

Murine model

This study used 40–45 week old apoE$^{-/-}$ mice (Jackson Laboratories) fed a high cholesterol diet (HCD, Harlan; 0.2% total cholesterol, 5 mice received HCD enriched with 0.01% wt/wt of atorvastatin[19]). These mice develop atherosclerotic lesions that resemble human disease; and although plaque rupture is not frequently reported, monocytes, macrophages and foam cells are present and produce proteases (reviewed in ref[20]). The accentuated inflammation in the aortic root has been used as a model system in several other imaging studies.[15, 21, 22] For determination of cholesterol levels, a blood sample of 500 μL was collected at the time of sacrifice and serum assayed for cholesterol by colorimetry (Raichem). The institutional subcommittee on research animal care approved all animal studies.

Blood half life of PS-5, PS-25 and PS-40

To determine the blood half-life of PS-5, PS-25 and PS-40, mice received an IV injection of 5 nanomoles of the agent via tail vein (6 C57BL/6 mice and also in 3–5 apoE$^{-/-}$ mice per agent). Bilateral retro-orbital bleeds were performed immediately and 2, 4, 8, 24 and 48 hours after injection. 50 μl of blood was drawn from alternating orbita using non-heparinized microcapillary tubes and collected into 50 μl of heparin. Equal volumes of heparinized blood and DMSO were incubated to activate the probe. Fluorescence of blood samples was then measured on a home built system (excitation/emission 680/700 nm).

Macroscopic ex vivo fluorescence reflectance imaging

Aortas were harvested 24 hours after injection of respective sensor and imaged with a fluorescence microscope at 4x magnification (OV-110, Olympus). Six apoE$^{-/-}$ mice were injected with PS-5, 4 with PS-25 and 3 with PS-40. In addition, 3 wild type mice on normal diet and 3 wild type mice that have been fed a diet high in cholesterol for 10 weeks were injected with each sensor. Two apoE$^{-/-}$ mice were co-injected with either PS-5 or PS-40 and in addition with a version of PS-25 that was synthesized with a spectrally resolved fluorochrome (VT750) to compare the regional activation profile of sensors. Light and near infrared fluorescence (NIRF) images were obtained in the 680 and 750 nm channels.

FMT-CT

We performed FMT-CT imaging at 680/700 nm excitation/emission wavelength in cohorts of mice at 2, 4, 8, 24 and 48 hours after injection of 5 nmol of respective PS using an FMT 2500 system (VisEn Medical) with an isotropic resolution of 1 mm. Each sensor was injected into 6–7 apoE$^{-/-}$ mice, 4–5 wild type mice on normal diet, and 3 wild type mice on high cholesterol diet. PS-40 was also injected into 5 apoE$^{-/-}$ mice treated with atorvastatin. Mice were anesthetized (Isoflurane 1.5 %, O2 2L/min) during imaging with a gas delivery system integrated into the multimodal imaging cartridge that holds the mouse during FMT and CT imaging. This cartridge facilitates co-registration of FMT to CT data through fiducial landmarks on its frame. Total imaging time for FMT acquisition was typically 5–8 minutes. Data were post-processed using a normalized Born forward equation to calculate three-dimensional fluorochrome concentration distribution. CT angiography immediately followed FMT to robustly identify the aortic root as the region of interest. The imaging cartridge lightly compressed the anesthetized mouse between optically translucent windows and thereby prevented motion during transfer to the CT (Inveon PET-CT, Siemens). The CT x-ray source operated at 80 kVp and 500 μA with an exposure time of 370 – 400 ms to acquire 360 projections. The effective 3D CT resolution was 80 μm isotropic. During CT acquisition, Isovue-370 was infused at 55 μL/min through a tail vein catheter. The CT reconstruction protocol performed bilinear interpolation, used a Shepp-Logan filter, and scaled pixels to Hounsfield units. We then imported data into OsiriX (The OsiriX foundation) to co-register FMT and CT images. Fiducials on the imaging cartridge were visualized and tagged in FMT

and CT images with point markers to define their XYZ coordinates. Using these coordinates, data were re-sampled, rotated and translated to match the image matrices, and finally displayed in one hybrid image.

Microscopy

For comparison of PS activation to microscopic cathepsin B distribution in plaques, aortic roots were excised from 2 apoE$^{-/-}$ mice per sensor and embedded in OCT (Sakura). Serial 6 μm thick transversal sections were collected and stained with a primary antibody targeting the model protease cathepsin B (Santa Cruz), a biotinylated secondary antibody (Vector), streptavidin-texas red (Amersham) and mounting medium with DAPI (Vector). Cathepsin B signal and activation of the PS were assessed using an epifluorescence microscope (Eclipse 80i, Nikon).

Flow cytometry

To investigate the cellular signal contributions for each protease sensor, we assessed blood and aortic tissue fluorescence 24 hours after injection of PS-5, PS-25 and PS-40 into 1 apoE$^{-/-}$ mice per sensor. ApoE$^{-/-}$ mice were sacrificed and blood and aortas prepared as described previously. [9] For visualization of macrophages, monocytes, and neutrophils, cells were incubated with a cocktail of monoclonal antibodies against T cells (CD90-PE), B cells (B220-PE), NK cells (DX5-PE and NK1.1-PE), granulocytes (Ly-6G-PE), myeloid cells (CD11b-APC), macrophages/dendritic cells (F4/80-biotin-Strep-PerCP, I-A^{b}-biotin-Strep-PerCP and CD11c-biotin-Strep-PerCP, all from BD Biosciences,). Data were acquired on an LSRII (BD Biosciences) with 670/LP and 695/40 filter configuration to detect PS activation.

Quantitative PCR

As an independent validation, the translation of mRNA encoding cathepsin B was measured in apoE$^{-/-}$ mice with and without atorvastatin therapy. Multiplex quantitative PCR was performed on triplicate samples using Applied Biosystems TaqMan® Gene Expression Assays and the 7500 Fast Real-Time PCR System. Primers were obtained from Applied Biosystems (Mm01310506_m1). Results were normalized to glyceraldehyde-3-phosphate dehydrogenase (GAPDH).

Statistics

Results are expressed as mean±SEM. The data were tested for normality using the Kolmogorov-Smirnov test, and for equality of variances using the F test. Data were compared using the unpaired two-sided t-test. If either normality or equality of variances were rejected, the nonparametric Mann-Whitney test was used. For multiple comparisons, we used ANOVA followed by Bonferroni post test. The significance level in all tests was 0.05.

Results

In vitro characteristics of sensors

Figure 1A–B provides an overview of the structure and characterization of the three differently sized protease sensors. HPLC analysis confirmed calculated sizes of the sensors (Fig. 1C). The overall fluorescence intensity after activation was comparable for the three probes (Fig. 1D, E). However, PS-40 was quenched most efficiently likely due to its specific design in which multiple fluorochromes were attached to the nanoparticle (Fig. 1D). In vitro assaying provided cleavage efficiency for a number of enzymes involved in plaque destabilization (Fig. 1F). Highest fluorescence intensity was observed after incubation with cathepsin B.

Pharmacokinetics favor PS-40 for in vivo FMT

We first measured the blood half life of the three PS to investigate impact of agent size on the clearance from the blood pool. Each sensor was injected into 6 wild type mice, and blood was drawn at several time points. For PS-5 and PS-40, a one-compartment model best described the signal behavior over time. For PS-25, a two-compartment model was used because it better described the data points and a one-compartment model did not converge. The shortest blood half life was observed for PS-5, followed by PS-25 and PS-40 (5.5 ± 0.5 hrs, 13.1 ± 1.6 hrs, 19.0 ± 2.2 hrs, Fig. 2A). Blood half life was also determined in apoE$^{-/-}$ mice for each sensor. Values were in the 95% confidence interval of wild type values (6.3 hrs for PS-5, 13.7 hrs for PS-25, 18.9 hrs for PS-40).

Using the measured blood half life and reported values for the rate of probe uptake, the concentration of active dye in the aorta was modeled in-silico as a function of time (Fig. 2B and online supplement). PS-5 reached its maximum signal earliest due to its rapid clearance from the plasma. PS-40 had a longer blood half-life, gave a higher maximum signal, but took longer to accumulate. The clearance rate of PS-25 from the blood fit a biexponential decay model, as expected for hydrophilic molecules of this size.[23] The plasma half life of PS-40 was predicted to give rise to the highest signal intensity. Therefore, even longer half lives were simulated to see if larger gains could be achieved. Modeling results indicate that these longer half life agents have diminishing returns. For instance, a 10-fold increase in the clearance half life would be required to double the signal intensity in plaque. These slow kinetics would likely increase the background signal. Given the marginal benefits of developing a sensor with such a long half life, we did not pursue its synthesis.

Ex vivo FRI shows activation profile in plaques

We then injected PS-5, PS-25 and PS-40 into wild type mice on normal and high fat diet and apoE$^{-/-}$ mice. Twenty four hours later, mice were sacrificed, their aortas excised, and ex vivo fluorescence in atherosclerotic plaques and non-diseased vessel wall was compared. Activation of all sensors was higher in atherosclerotic lesions than in undiseased tissue (Fig. 2C, D). No lesions were observed in wild type mice on high cholesterol diet. In apoE$^{-/-}$ mice, plaque signal intensities were highest for PS-40, followed by PS-25 (Fig. 2C, D). However, when the plaque target-to-background ratio was compared, diagnostic values were observed for all three sensors, ranging from 4.76 ± 0.56 for PS-5 to 7.13 ± 1.36 for PS-40 (Fig. 2E). In contrast, control, wild type mice on normal and high fat diet showed an up to 6-fold lower target (aortic root) to background (descending aorta) ratio (Fig. 2E, $p<0.05$ vs. apoE$^{-/-}$). To investigate the regional activation profile of the 3 sensors, apoE$^{-/-}$mice were coinjected with PS-5 or PS-40 and PS-25 derivatized with a higher wavelength fluorochrome for spectrally resolved imaging. The activation profile was comparable with small

In vivo FMT-CT detects activation in aortic root

We next followed activation of the three probes by serial in vivo FMT-CT imaging. The concept of hybrid imaging is illustrated in apoE$^{-/-}$ mice in Fig. 3A–C. Fiducial markers were readily identified on the imaging cartridge in both modalities and allowed co-registration of data sets in an automated fashion. CT angiography allowed to identify the aortic root as the vascular territory with highest protease activity. Representative 2 and 3 dimensional data sets are shown in Fig. 3D–U. CT imaging also showed vascular calcifications (Fig. 3G and 3H). The in vivo signal time course was followed for each protease sensor over time and is depicted in Fig. 3V. Highest fluorescence concentrations were measured for PS-40 at 24 hours after injection, followed by PS-25 (Fig. 3W). PS-5 had the fastest wash-in and wash-out kinetics. Much lower signals were observed in mice without atherosclerosis, and all three sensors detected protease activity in vivo. However, PS-40 showed the highest fluorescence in plaques.

Immunoreactive protease presence colocalizes with PS activation

The microscopic signal distribution was compared to immunoreactive staining for cathepsin B (Fig. 4). There was good co-localization of probe activation with immunofluorescent cathepsin B signal.

Cellular target profile by flow cytometry

Flow cytometric profiling identified monocyte/ macrophages as the dominant cellular signal source for all sensors in plaques (Fig. 5). The highest mean fluorescence intensity was observed for PS-40. Some uptake of PS-5 was also seen in neutrophils accumulating in the aortic tissue. Lymphocytes and cells that constitute the aortic wall, e.g. endothelial cells and fibroblasts showed very low signal. In the blood, we observed considerable differences in signal profiles for respective sensors. Whereas there was virtually no activation of PS-5, we observed intermediate and high fluorescence signals in monocytes after injection of PS-25 and PS-40, respectively (Fig. 5).

PS-40 detects therapy effects in vivo

Having identified PS-40 as the sensor with superior sensitivity, we further explored its use for non-invasive detection of reduced inflammation in plaque after statin therapy. Atorvastatin is known to reduce the recruitment of inflammatory monocytes, in part through reduction of VCAM-1 expression.[22] These cells and their lineage descendants are the primary source of plaque cathepsin[1, 10] and together, dominate activation of PS-40 in vivo. Thus, we used FMT-CT for imaging of apoE$^{-/-}$ mice treated with atorvastatin. 24 hours after injection of PS-40, (i.e., at the peak of protease signal intensity), we observed a 2.6-fold reduced FMT signal in the aortic root in treated mice ($p < 0.05$, Fig. 6 A-C). These data corroborated with ex vivo FRI of excised aortas (Fig. 6D–E) and with quantitative PCR for expression of the model protease cathepsin B (Fig. 6F). As expected in apoE$^{-/-}$ mice, cholesterol blood levels were mildly reduced by atorvastatin treatment (Fig. 6G).

Discussion

Fluorescence molecular tomography is an emerging modality increasingly used in preclinical imaging.[14] Here we addressed two obstacles that have limited the utility of FMT to image murine models of atherosclerosis. First, we used an imaging cartridge in free space FMT to merge molecular data with detailed anatomic information provided by high resolution CT angiography. Second, we show that sensitivity, target to background ratio and the pharmacokinetic profile of nano-engineered fluorescent probes can be specifically tailored to meet the demands of individual imaging applications.

Combination of molecular sensing by FMT with anatomical CT imaging in a hybrid set-up was achieved based on landmark-facilitated image co-registration. FMT imaging was immediately followed by CT, while the anesthetized mouse was transferred in a multimodal imaging cartridge that i) ensured a constant position of the mouse and ii) provided the fiducials for co-registration on its frame. An optimized CT angiography protocol provided excellent anatomic information of murine vasculature and visualized calcified plaque. The hybrid approach enhanced the quantitative robustness of in vivo FMT imaging because the region of interest for signal quantification was chosen based on anatomic detail provided by CT, in this case the aortic root, rather than signal intensity. Re-identification of this landmark in serial imaging allowed us to follow protease activity in individual lesions over time. We anticipate that this will prove particularly useful for investigations of experimental anti-inflammatory therapies.

The design for protease sensors closely positions fluorochromes on a nano-scaffold to induce auto-quenching.[13] The nanomaterial includes polypeptides as substrate sequences for proteases. In this study, an oligo-L-lysine peptide sequence was used that is primarily cleaved by cathepsins. In the presence of the active protease, cleavage occurs and fluorochromes are liberated and unquenched and therefore can emit fluorescence. This design harbors a powerful amplification strategy, since one moiety of active enzyme can cleave and activate multiple targets. While using an identical activation mechanism, we modified the size of the sensors and the number of attached fluorochromes, and in the case of PS-40, used an iron oxide nanoparticle as a central core, giving rise to unique properties each agent exhibited.

PS-40 had the longest plasma half life and slowest wash out from atherosclerotic plaques. The dextran-coated iron oxide core, which is comparably large in size (40 nm), increased the blood half life and likely promoted cellular retention of activated probe in target tissue after interaction with proteases, whereas smaller cleavage products of PS-25 and PS-5 were washed out faster. The function of PS-40's core as a ‘cellular anchor’ for activated fluorochromes resulted in high signal intensities in atherosclerotic plaques in and ex vivo. As a consequence, the improved sensitivity of PS-40 facilitated non-invasive detection of protease activity modulated by therapy, highlighting the value of FMT-CT for preclinical R&D efforts.

Fluorescence penetrates a limited depth of tissue.[7] Therefore, intravascular sensing of protease activity has been performed successfully in animal models,[24] with the aim of translating identification of inflamed plaques into the cath lab. For this application, minimized blood background fluorescence is essential to facilitate sensing of signal in the vessel wall. Flow cytometric analysis showed that PS-5 had minimal uptake into circulating leukocytes. In addition, PS-5 exhibited fast kinetics that would allow for clinically desirable rapid injection-imaging sequences. Another application that benefits from the low blood background signal afforded by PS-5 is flow cytometric profiling of cell suspensions dislodged from solid tissues.[8, 9, 25] While tissue is usually rinsed prior to enzymatic digestion, some contamination with blood is inevitable. As PS-5 showed no uptake into circulating blood cells, it minimizes this interference.

We used pharmacokinetic data to model in vivo signal in atherosclerotic plaques. The model accounted for agent dose, plasma clearance, pinocytosis rate in activated macrophages, macrophage plaque density, and probe retention in the plaque. There was good agreement between the model predictions and experimental data, providing evidence that the mechanisms used in the model determine the probe behavior in vivo. In-silico experimentation indicated that further increases in plasma half-life have diminishing returns on signal intensity and would increase the necessary delay between injection and imaging at the time of maximum plaque signal. The mechanism-based model can be used to examine any probe design, including addition of targeting ligands or scale-up from mouse to man without the requirement for allometric scaling or empirical assumptions.

In summary, we show that nanotechnology-enabled tailoring of protease sensors optimizes imaging agent design for specific applications. The use of a nanoparticulate ‘cell anchor’ for PS-40 enhanced sensitivity and enabled non-invasive FMT-CT imaging of treatment effects. We anticipate that the use of this sensor in conjunction with hybrid FMT-CT imaging will catalyze quantitative in vivo plaque interrogation in mouse models of atherosclerosis frequently used in basic research and drug development.

Supplementary Material

Refer to Web version on PubMed Central for supplementary material.

Acknowledgements

The authors acknowledge the help of the CSB Mouse Imaging Program (Edmund Keliher, PhD) and Wael Yared, PhD for helpful discussions. Yoshiko Iwamoto, BS, is acknowledged for help with histology. Jihong Wang, PhD is acknowledged for performing in vitro activation experiments.

Funding sources

This work was funded in part by R24-CA92782 and UO1-HL08073 (to RW) and by the American Heart Association 0835623D (to MN).

References

1. Libby P. Inflammation in atherosclerosis. Nature 2002;420:868–874. [PubMed: 12490960]
2. Sanz J, Fayad ZA. Imaging of atherosclerotic cardiovascular disease. Nature 2008;451:953–957. [PubMed: 18288186]
3. Falk E, Shah PK, Fuster V. Coronary plaque disruption. Circulation 1995;92:657–671. [PubMed: 7634481]
4. Zhang J, Nie L, Razavian M, Ahmed M, Dobrucki LW, Asadi A, Edwards DS, Azure M, Sinusas AJ, Sadeghi MM. Molecular imaging of activated matrix metalloproteinases in vascular remodeling. Circulation 2008;118:1953–1960. [PubMed: 18936327]
5. Schafers M, Riemann B, Kopka K, Breyholz HJ, Wagner S, Schafers KP, Law MP, Schober O, Levkau B. Scintigraphic imaging of matrix metalloproteinase activity in the arterial wall in vivo. Circulation 2004;109:2554–2559. [PubMed: 15123523]
6. Amirbekian V, Aguinaldo JG, Amirbekian S, Hyafil F, Vucic E, Sirol M, Weinreb DB, Le GreneurS, Lancelot E, Corot C, Fisher EA, Galis ZS, Fayad ZA. Atherosclerosis and matrix metalloproteinases: experimental molecular MR imaging in vivo. Radiology 2009;251:429–438. [PubMed: 19224894]
7. Ntziachristos V, Tung CH, Bremer C, Weissleder R. Fluorescence molecular tomography resolves protease activity in vivo. Nat Med 2002;8:757–760. [PubMed: 12091907]
8. Nahrendorf M, Sosnovik DE, Waterman P, Swirski FK, Pande AN AikawaE, Figueiredo JL, Pittet MJ, Weissleder R. Dual channel optical tomographic imaging of leukocyte recruitment and protease activity in the healing myocardial infarct. Circ Res 2007;100:1218–1225. [PubMed: 17379832]
9. Nahrendorf M, Swirski FK, Aikawa E, Stangenberg L, Wurdinger T, Figueiredo JL, Libby P, Weissleder R, Pittet MJ. The healing myocardium sequentially mobilizes two monocyte subsets with divergent and complementary functions. J Exp Med 2007;204:3037–3047. [PubMed: 18025128]
10. Liu J, Sukhova GK, Sun JS, Xu WH, Libby P, Shi GP. Lysosomal cysteine proteases in atherosclerosis. Arterioscler Thromb Vasc Biol 2004;24:1359–1366. [PubMed: 15178558]
11. Chen J, Tung CH, Mahmood U, Ntziachristos V, Gyurko R, Fishman MC, Huang PL, Weissleder R. In vivo imaging of proteolytic activity in atherosclerosis. Circulation 2002;105:2766–2771. [PubMed: 12057992]
12. Weissleder R, Pittet MJ. Imaging in the era of molecular oncology. Nature 2008;452:580–589. [PubMed: 18385732]
13. Weissleder R, Ntziachristos V. Shedding light onto live molecular targets. Nat Med 2003;9:123–128. [PubMed: 12514725]
14. Sinusas AJBF, Nahrendorf M, Epstein FH, Wu JC, Villanueva FS, Fayad ZA, Gropler RJ. Multimodality Cardiovascular Molecular Imaging, Part I. Circ Cardiovasc Imaging 2008;1:244–256.
15. Nahrendorf M, Zhang H, Hembrador S, Panizzi P, Sosnovik DE, Aikawa E, Libby P, Swirski FK, Weissleder R. Nanoparticle PET-CT imaging of macrophages in inflammatory atherosclerosis. Circulation 2008;117:379–387. [PubMed: 18158358]
16. Rudd JH, Myers KS, Bansilal S, Machac J, Pinto CA, Tong C, Rafique A, Hargeaves R, Farkouh M, Fuster V, Fayad ZA. Atherosclerosis Inflammation Imaging with 18F-FDG PET: Carotid, Iliac, and Femoral Uptake Reproducibility, Quantification Methods, and Recommendations. J Nucl Med 2008;49:871–878. [PubMed: 18483100]
17. Rudd JH, Warburton EA, Fryer TD, Jones HA, Clark JC, Antoun N, Johnstrom P, Davenport AP, Kirkpatrick PJ, Arch BN, Pickard JD, Weissberg PL. Imaging atherosclerotic plaque inflammation

with [18F]-fluorodeoxyglucose positron emission tomography. Circulation 2002;105:2708–2711. [PubMed: 12057982]

18. Weissleder R, Kelly K, Sun EY, Shtatland T, Josephson L. Cell-specific targeting of nanoparticles by multivalent attachment of small molecules. Nat Biotechnol 2005;23:1418–1423. [PubMed: 16244656]
19. Verschuren L, Kleemann R, Offerman EH, Szalai AJ, Emeis SJ, Princen HM, Kooistra T. Effect of low dose atorvastatin versus diet-induced cholesterol lowering on atherosclerotic lesion progression and inflammation in apolipoprotein E*3-Leiden transgenic mice. Arterioscler Thromb Vasc Biol 2005;25:161–167. [PubMed: 15514207]
20. Meir KS, Leitersdorf E. Atherosclerosis in the apolipoprotein-E-deficient mouse: a decade of progress. Arterioscler Thromb Vasc Biol 2004;24:1006–1014. [PubMed: 15087308]
21. Itskovich VV, Choudhury RP, Aguinaldo JG, Fallon JT, Omerhodzic S, Fisher EA, Fayad ZA. Characterization of aortic root atherosclerosis in ApoE knockout mice: high-resolution in vivo and ex vivo MRM with histological correlation. Magn Reson Med 2003;49:381–385. [PubMed: 12541260]
22. Nahrendorf M, Jaffer FA, Kelly KA, Sosnovik DE, Aikawa E, Libby P, Weissleder R. Noninvasive vascular cell adhesion molecule-1 imaging identifies inflammatory activation of cells in atherosclerosis. Circulation 2006;114:1504–1511. [PubMed: 17000904]
23. Bazin-Redureau M, Pepin S, Hong G, Debray M, Scherrmann JM. Interspecies scaling of clearance and volume of distribution for horse antivenom F(ab')2. Toxicol Appl Pharmacol 1998;150:295–300. [PubMed: 9653060]
24. Jaffer FA, Vinegoni C, John MC, Aikawa E, Gold HK, Finn AV, Ntziachristos V, Libby P, Weissleder R. Real-time catheter molecular sensing of inflammation in proteolytically active atherosclerosis. Circulation 2008;118:1802–1809. [PubMed: 18852366]
25. Nahrendorf MSD, French B, Swirski FK, Bengel F, Sadeghi MM, Lindner JR, Wu JC, Kraitchman DL, Fayad ZA, Sinusas AJ. Multimodality Cardiovascular Molecular Imaging, Part II. Circ Cardiovasc Imaging 2009;2:56–70.

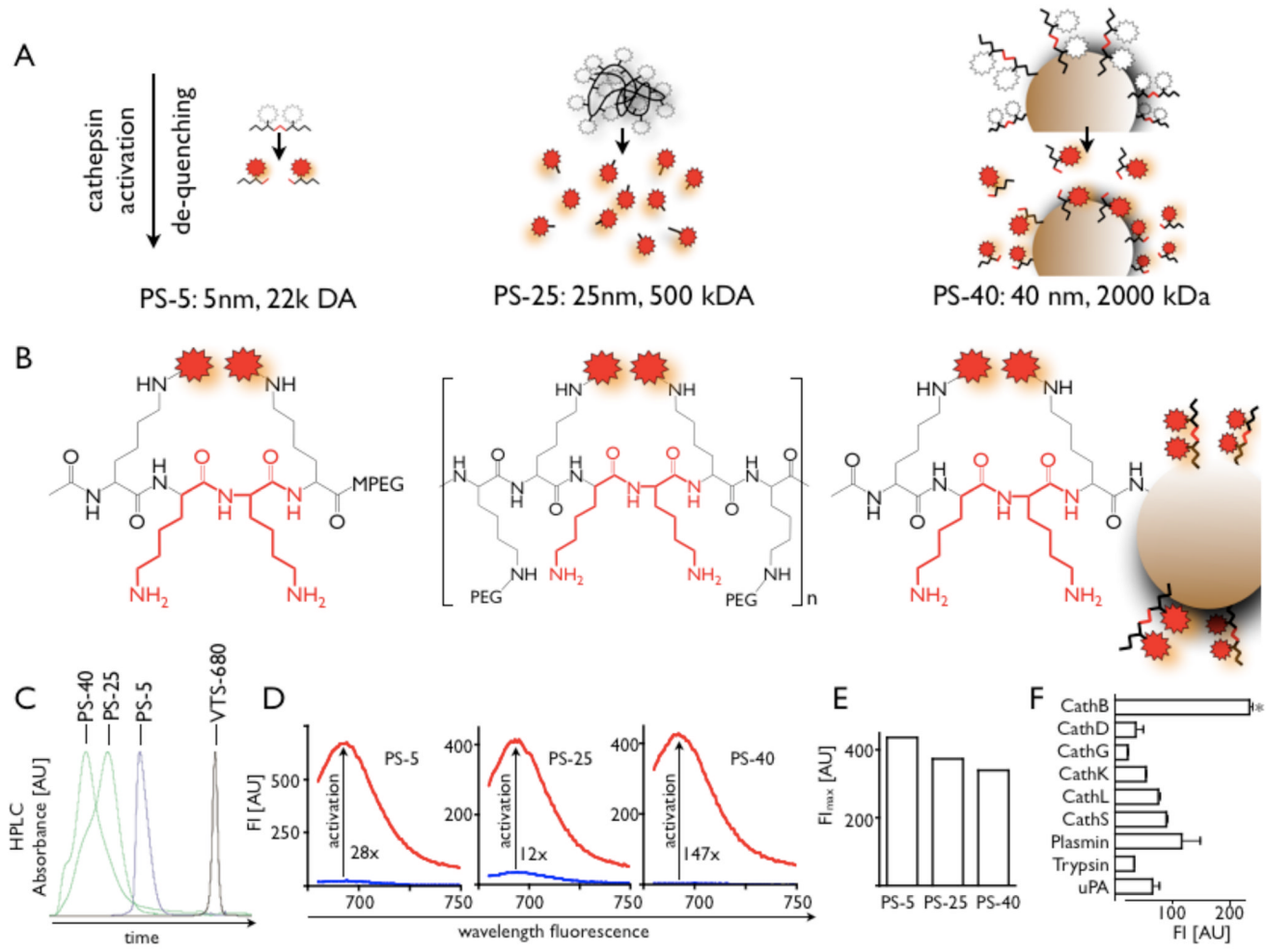

Figure 1. Probe design and characterization

A: scheme of three different probe designs (PS: protease sensor). White and red stars depict quenched and unquenched fluorochromes, respectively.

B: Structure of protease cleavage site on respective PS.

C: Size exclusion HPLC (SEC) of PS-5, PS-25 and PS-40 and the used fluorochrome as a low molecular weight (1 kDa) reference reflects differences in size. The largest sensor, PS-40, is eluted first, and the smallest last.

D: Fluorescence of inactive (blue) and activated sensors shows the emission peak and the activation after incubation with trypsin. Sufficient quenching is achieved for all three sensors, however, PS-40 is most silent in its inactive form and has therefore the highest increase in fluorescence when activated.

E: Comparison of fluorescence intensity of trypsin activated probes at equal concentrations in PBS.

F: In vitro activation of PS-25 with different enzymes. The highest activation efficacy was found for incubation with cathepsin B.

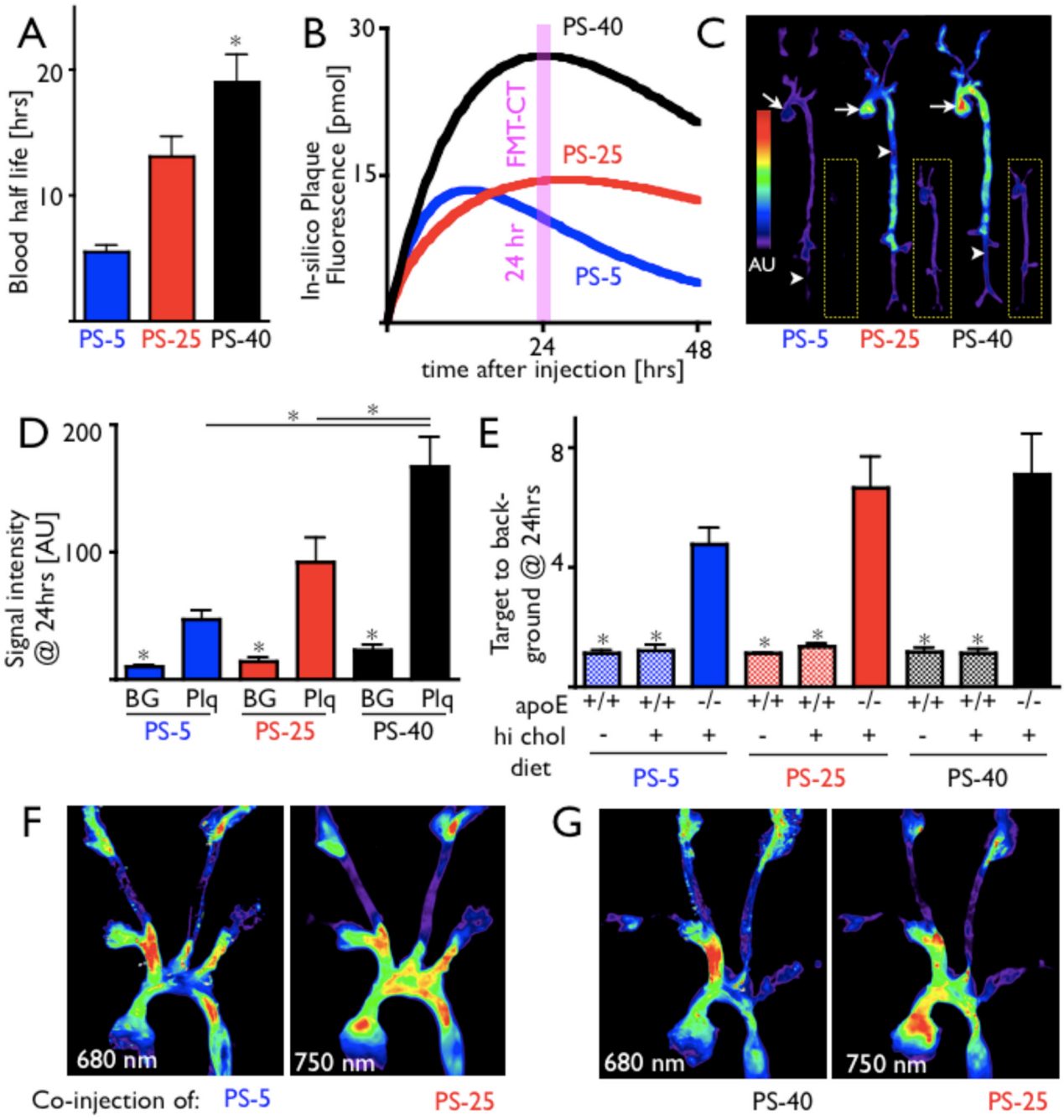

Figure 2. Pharmacokinetics and ex vivo imaging of activation

A: Blood half life of protease sensors.

B: Modeling results for protease sensors of different size and design. The fluorescence inside inflamed atherosclerotic plaques was simulated taking into account pharmacokinetics, cellular uptake and wash in/out of target tissue, and suggests that PS-40 reaches the highest fluorescence intensity inside plaques and has slowest wash out kinetics.

C–E: Fluorescence reflectance imaging (FRI) of excised aortas from apoE$^{-/-}$ mice and wild type mice (insets in panel C) 24 hours after injection of respective protease sensor. The signal intensity was significantly higher in plaque (Plq, arrow) when compared to vascular territories without lesions (background, BG, arrowhead) and highest for PS-40 (D). However, the target

to background ratio, which normalizes fluorescence in plaques to signal in non-diseased vascular territory, is sufficiently higher in apoE$^{-/-}$ than in wild type mice on normal and on high fat diet for all three sensors (E). * $p < 0.05$.

F and G: Dual-channel FRI of aortas from apoE$^{-/-}$ mice that were co-injected with spectrally resolved protease sensors. For this experiment, a higher wavelength version of PS-25 was used (excitation/emission 750/780). Overall similar activation mapping was observed, with small regional differences between respective sensors.

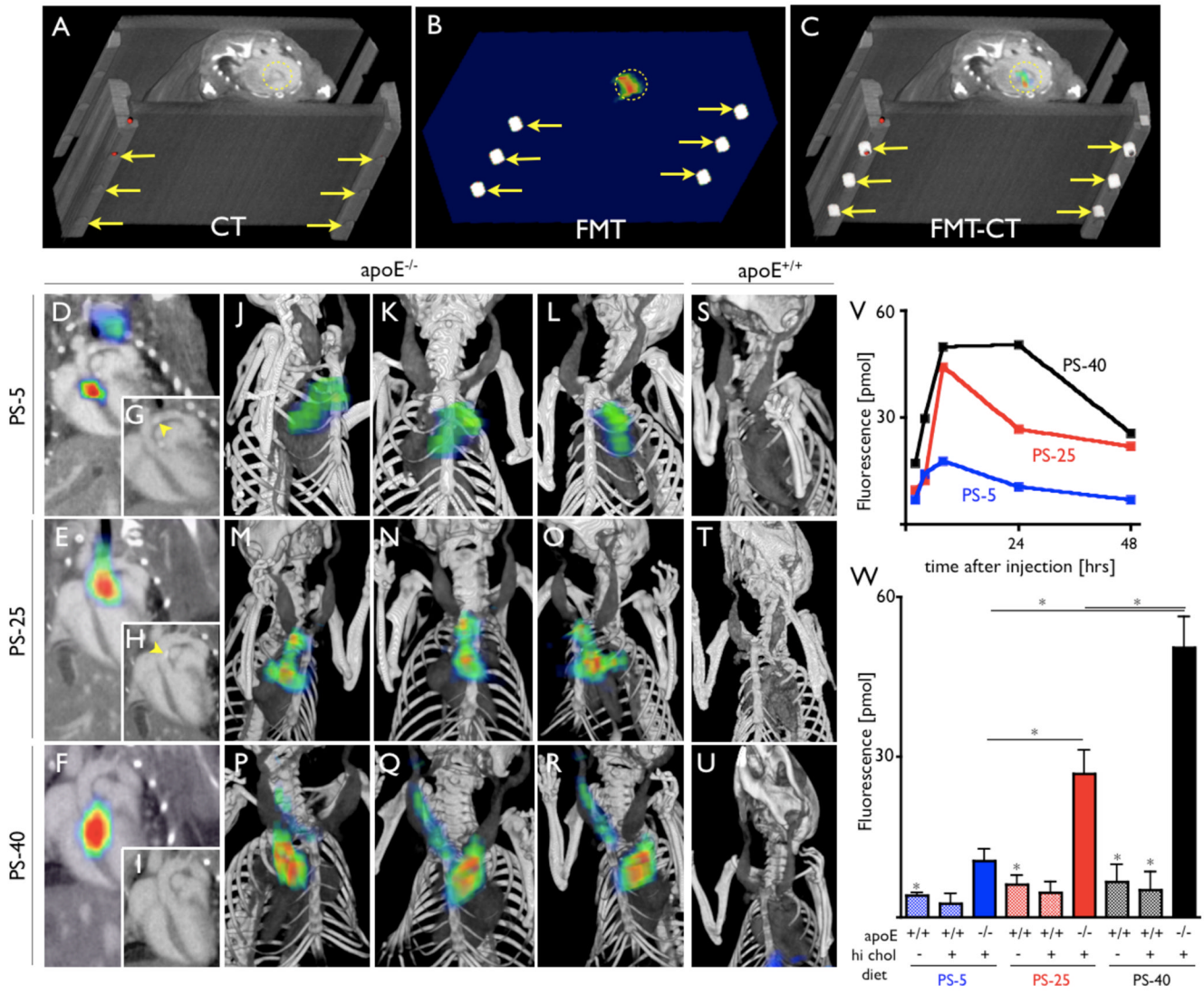

Figure 3. In vivo FMT-CT

In vivo Fluorescence Molecular Tomography-Computed Tomography imaging (FMT-CT). A–C: Image co-registration is based on fiducial landmarks (arrows) that are incorporated into the animal holder and are identifiable on CT (A) and FMT (B). The software co-aligns these fiducials to create a hybrid data set (C). Fluorescence signal in the aortic root of an apoE$^{-/-}$mouse is encircled.

D–F: 2-dimensional FMT-CT long axis views of apoE$^{-/-}$ mice injected with respective protease sensors. Fluorescence signal is observed in the aortic root and arch, regions with high plaque load and high ex vivo fluorescence signal (as shown in Figure 2).

G–I: CT only views of D–F. Arrow heads depict vascular calcification, likely colocalizing with plaques.

J–R: 3-dimensional maximum intensity projection of hybrid data sets show skeletal and vascular anatomy and the distribution of fluorescence signal. Most signal is observed in the root and arch, however, Q and R show additional activation of the protease sensor in the carotid artery, also a region predisposed to atheroma build-up in this model. S-U: FMT-CT after injection of respective sensor into wild type mice. V: Fluorochrome concentration reflecting

protease activity plotted over time. W: Protease activity 24 hours after injection of sensors. *p<0.05.

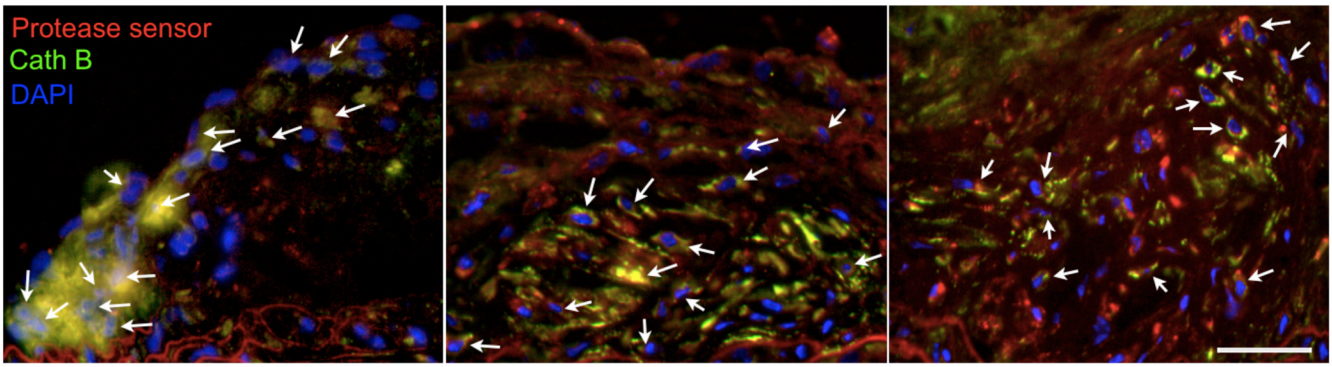

Figure 4. Microscopic mapping of probe activation

Immunofluorescence microscopy of cathepsin B presence (green, emission 620nm), DAPI-stained DNA in cell nuclei (blue, emission 460nm) and protease sensor activation (red, emission 700nm) shows colocalisation in atherosclerotic plaques (yellow, arrows). Left panel shows histology from apoE$^{-/-}$ mouse injected with PS-5, middle PS-25, and right PS-40. The error bar denotes 50μm.

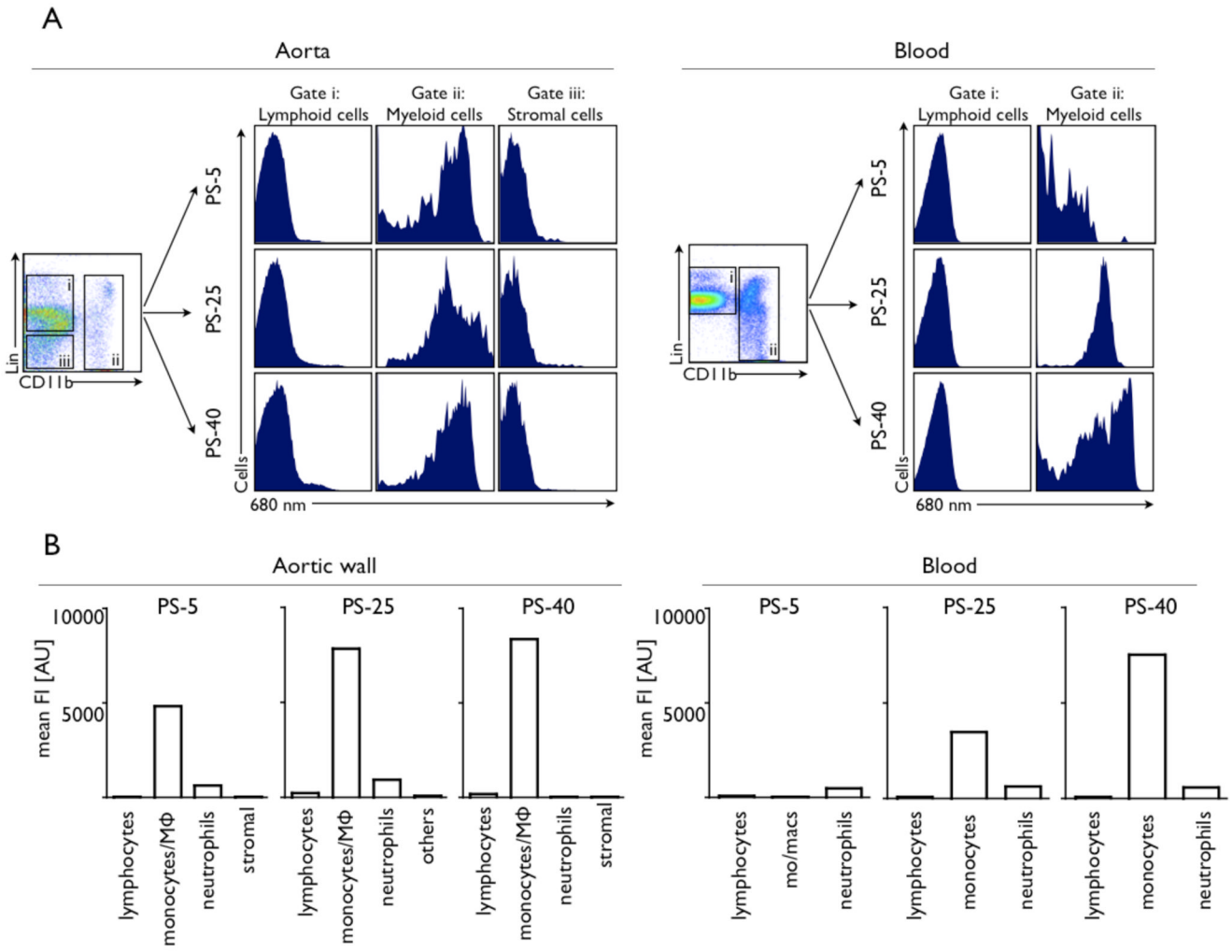

Figure 5. Flow cytometric profiling of cellular signal contributions

Flow cytometric profiling of cellular signal contributions in liquified aortas and background fluorescence in the blood 24 hours after injection of protease sensors into 3 age-matched apoE$^{-/-}$ mice.

A: Incubation of cell suspensions with an antibody cocktail enabled multicolor flow cytometric analysis of lymphoid cells, myeloid cells including monocytes/macrophages and neutrophils, and other cells, including stromal cell of the aortic wall. Histograms for these cell types show the signal intensity in the protease sensor channel, which is dominated by myeloid cells in the aorta for all sensors. In the blood, marked differences can be observed. While there is hardly any blood signal after injection of PS-5, myeloid cell signal is observed after injection of PS-25 and even more so for PS-40.

B: Mean fluorescence intensity per cell type. Monocyte/macrophages are the dominant cellular signal source for all 3 sensors. The highest mean fluorescence intensity per cell is observed after injection of PS-40.

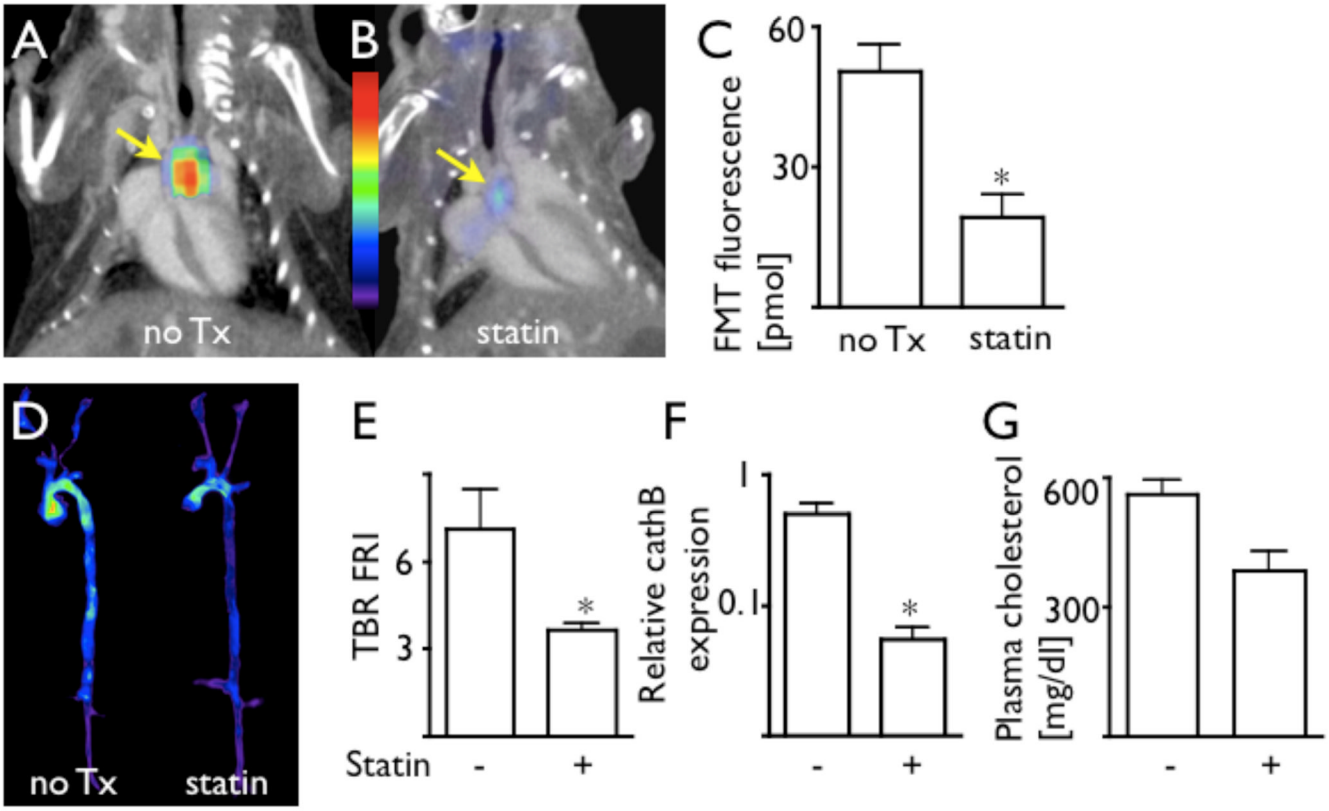

Figure 6. FMT-CT detection of therapy with PS-40

The protease sensor with the highest sensitivity, PS-40, was used in a therapy trial to investigate its potential as a non-invasive imaging biomarker in drug development.

A–B: FMT-CT data sets in respective treatment groups.

C: Fluorescence activity in the aortic root measured by FMT, 24 hours after injection of PS-40. The protease sensor detected effects of atorvastatin treatment. *$p<0.05$.

D–E: Ex vivo fluorescence reflectance imaging of excised aortas corroborated in vivo FMT data. *$p<0.05$.

F: Quantitative PCR analysis showed lower translation of cathepsin B in apoE$^{-/-}$ treated with atorvastatin, confirming the imaging data. *$p<0.05$.

G: Plasma cholesterol levels in respective trial groups.